TECHNICAL ARTICLE

Crystal structure of nilotinib, $C_{28}H_{22}F_3N_7O$

James A. Kaduk,[1,a] Kai Zhong,[2] Amy M. Gindhart,[2] and Thomas N. Blanton[2]
[1]*Illinois Institute of Technology, 3101 S. Dearborn St., Chicago, Illinois 60616*
[2]*ICDD, 12 Campus Blvd., Newtown Square, Pennsylvania 19073-3273*

(Received 5 February 2015; accepted 21 May 2015)

The crystal structure of nilotinib has been solved and refined using synchrotron X-ray powder diffraction data, and optimized using density functional techniques. Nilotinib crystallizes in space group *P*1 (#1) with $a = 4.518\ 14(3)$, $b = 10.638\ 01(5)$, $c = 13.703\ 77(8)$ Å, $\alpha = 68.8607(4)$, $\beta = 82.1486(5)$, $\gamma = 84.1978(5)°$, $V = 607.62(1)$ Å^3, and $Z = 1$. The most prominent feature of the structure is two strong hydrogen bonds. These form chains with a graph set C1,1(13); the chains run along [111]. Several weak C–H···O hydrogen bonds also contribute to the packing. The powder pattern has been submitted to ICDD for inclusion in future releases of the Powder Diffraction File™. © *2015 International Centre for Diffraction Data.* [doi:10.1017/S0885715615000512]

Key words: nilotinib, Tasigna®, powder diffraction, Rietveld refinement, density functional theory

I. INTRODUCTION

Nilotinib hydrochloride monohydrate (Tasigna®) is an orally bioavailable derivative of imatinib. As a second-generation tyrosine kinase inhibitor, it is approved for the treatment of a type of blood cancer called Philadelphia chromosome positive chronic myeloid leukemia (Deremer *et al.*, 2008). The free-base phase (nilotinib) does not contain HCl or H_2O. The systematic name (CAS Registry Number 641571-10-0) is 4-methyl-*N*-[3-(4-methyl-1*H*-imidazol-1-yl)-5-(trifluoromethyl)phenyl]-3-[(4-pyridin-3-ylpyrimidin-2-yl)amino]benzamide. A two-dimensional molecular diagram of nilotinib is shown in Figure 1.

The presence of high-quality reference powder patterns in the Powder Diffraction File (PDF; ICDD, 2014) is important for phase identification, particularly by pharmaceutical, forensic, and law enforcement scientists. The crystal structures of a significant fraction of the largest dollar volume pharmaceuticals have not been published, and thus calculated powder patterns are not present in the PDF-4 databases. Sometimes experimental patterns are reported, but they are generally of low quality. This structure is a result of a collaboration among ICDD, Illinois Institute of Technology, Poly Crystallography Inc., and Argonne National Laboratory to measure high-quality synchrotron powder patterns of commercial pharmaceutical ingredients, include these reference patterns in the PDF, and determine the crystal structures of these active pharmaceutical ingredients (APIs).

Even when the crystal structure of an API is reported, the single crystal structure was often determined at low temperature. Most powder measurements are performed at ambient conditions. Thermal expansion (often anisotropic) means that the peak positions calculated from a low-temperature single crystal structure often differ significantly from those measured at ambient conditions. These peak shifts can result in failure of default search/match algorithms to identify a phase, even when it is present in the sample. High-quality reference patterns measured at ambient conditions are thus critical for easy identification of APIs using standard powder diffraction practices.

II. EXPERIMENTAL

Nilotinib commercial reagent was purchased from Carbosynth LLC (lot FN108311101) and was used as-received. The white powder was packed into a 1.5 mm diameter Kapton capillary, and rotated during the measurement at ~50 cycles s^{-1}. The powder pattern was measured at 295 K at beam line 11-BM (Lee *et al.*, 2008; Wang *et al.*, 2008) of the Advanced Photon Source at Argonne National Laboratory using a wavelength of 0.413 691 Å from 0.5° to 50° 2θ with a step size of 0.001° and a counting time of 0.1 s step^{-1}. The pattern was indexed on a primitive triclinic unit cell having $a = 4.5181$, $b = 10.6391$, $c = 13.7042$ Å, $\alpha = 68.862$, $\beta = 82.143$, $\gamma = 84.200°$, $V = 607.70$ Å^3, and $Z = 1$ using DICVOL06 (Louër and Boultif, 2007). With one molecule in the unit cell, the space group was assumed to be *P*1. A reduced cell search in the Cambridge Structural Database (Allen, 2002) yielded nine hits, but no structure for nilotinib.

A nilotinib cation was built and its conformation optimized using Spartan'14 (Wavefunction, 2013), and saved as a mol2 file. This file was converted into a Fenske–Hall *Z*-matrix file using OpenBabel (O'Boyle *et al.*, 2011). Preliminary attempts to solve the structure using this molecule, a chlorine atom, and an oxygen atom (water molecule) led to solutions in which the Cl and O were too close to the organic cation. (The authors originally believed that this sample was nilotinib hydrochloride monohydrate.) A direct methods solution using EXPO2013 (Altomare *et al.*, 2013) yielded no heavy atom. Accordingly, only a nilotinib molecule was used as a fragment to solve the structure using FOX (Favre-Nicolin and Černý, 2002). Much higher-quality solutions were obtained, and subsequent refinement confirmed that the sample was nilotinib. Chemical analysis indicated only traces of Cl (consistent with the NaCl detected during

[a]Author to whom correspondence should be addressed. Electronic mail: kaduk@polycrystallography.com

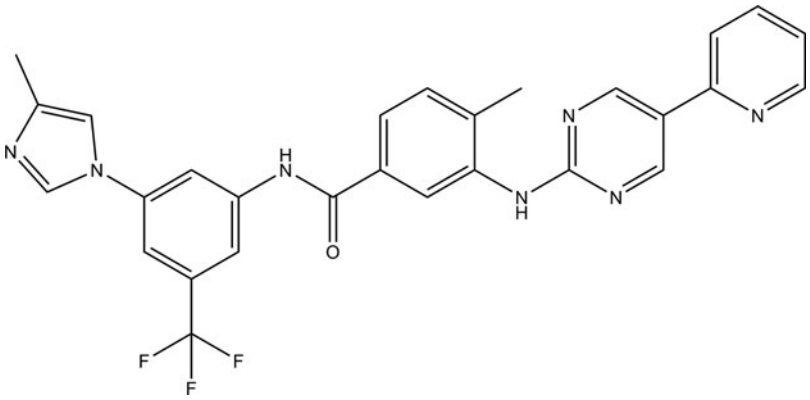

Figure 1. The molecular structure of nilotinib.

the refinement) and not the 6.3 wt% Cl expected for the hydrochloride, confirming that the sample was free base. Positions of the active hydrogens were deduced by an analysis of potential hydrogen bonding.

Rietveld refinement was carried out using the General Structure Analysis System (GSAS) (Larson and Von Dreele, 2004). Only the 2.0°–25°portion of the pattern was included in the refinement. The C1–C6 and C20–C25 benzene rings were refined as rigid bodies. All other non-H bond distances and angles were subjected to restraints, based on a Mercury/Mogul Geometry Check (Bruno *et al.*, 2004; Sykes *et al.*, 2011) of the molecule. The Mogul average and standard deviation for each quantity were used as the restraint parameters. The restraints contributed 4.00% to the final χ^2. Isotropic displacement coefficients were refined, grouped by chemical similarity. The hydrogen atoms were included in calculated positions, which were recalculated during the refinement. The U_{iso} of each hydrogen atom was constrained to be 1.3 × that of the heavy atom to which it is attached. The peak profiles were described using profile function #4 (Thompson *et al.*, 1987; Finger *et al.*, 1994), which includes the Stephens (1999) anisotropic strain broadening model. The background was modeled using a three-term shifted Chebyshev polynomial and an eight-term diffuse scattering (Debye) function, to model the scattering from the Kapton capillary and any amorphous component of the sample. A second-order spherical harmonic preferred orientation correction was included in the model. A few weak peaks not accounted for by nilotinib indicated the presence of NaCl (0.54 wt%), which was included in the refinement as a second phase.

Initial refinement of the model from FOX yielded an excellent refinement; $R_{wp} = 0.0708$, $R_p = 0.0545$, and $\chi^2 = 1.083$. The root-mean-square deviation of the non-hydrogen atoms was 0.290 Å, a little high, but within the range of correct structures (van de Streek and Neumann, 2014). However, we realized that rotating the C34–C39 C_5H_4N ring by 180° would result in a more-reasonable hydrogen bonding pattern. A density functional theory (DFT) geometry optimization of this second model yielded a structure 10.4 Kcal mole^{-1} lower in energy, and this structure was used as the basis for the final refinement. The final refinement of 130 variables using 23 081 observations (23 002 data points and 79 restraints) yielded the residuals $R_{wp} = 0.0717$, $R_p = 0.0559$, and $\chi^2 = 1.161$. The largest peak (1.12 Å from C18) and hole (2.02 Å from N29) in the difference Fourier map were 0.34 and −0.37 e Å^{-3}, respectively. The Rietveld plot is included as Figure 2. The largest errors are in the shapes of some of the low-angle peaks. These errors and some difficulty in

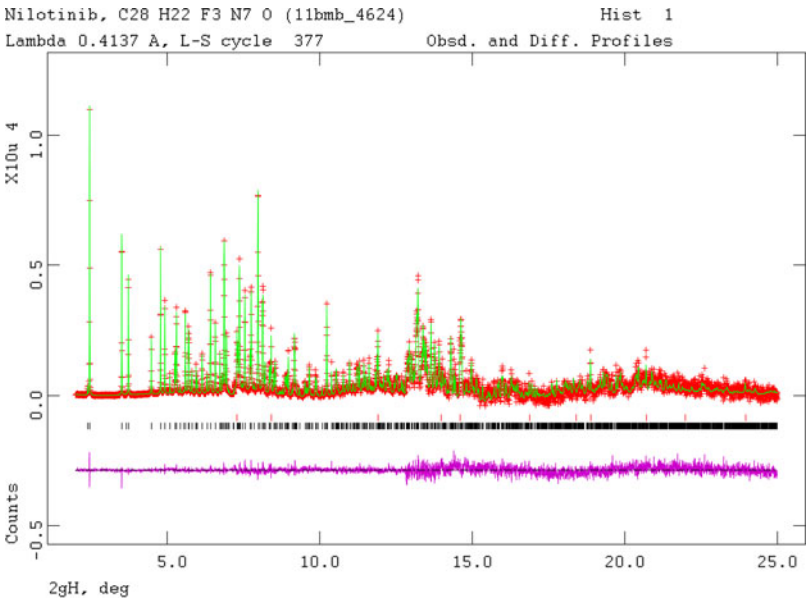

Figure 2. (Color online) The Rietveld plot for the refinement of nilotinib. The red crosses represent the observed data points, and the green line is the calculated pattern. The magenta curve is the difference pattern, plotted at the same vertical scales as the other patterns. The vertical scale has been multiplied by a factor of 5 for $2\theta > 7.2°$ and by a factor of 20 for $2\theta > 12.8°$.

https://doi.org/10.1017/S0885715615000512 Published online by Cambridge University Press

TABLE I. Rietveld refined crystal structure of nilotinib.

Crystal data	
$C_{28}H_{22}F_3N_7O$	$\beta = 82.1480\ (4)°$
$M_r = 529.53$	$\gamma = 84.1976\ (4)°$
Triclinic, $P1$	$V = 607.61(1)$ Å^3
$a = 4.518\ 13\ (2)$ Å	$Z = 1$
$b = 10.637\ 96\ (4)$ Å	Synchrotron radiation, $\lambda = 0.413\ 691$ Å
$c = 13.703\ 79\ (6)$ Å	Cylinder, $1.5 \times 1.5 \times 3.0$ mm^3
$\alpha = 68.8608\ (3)°$	
Refinement	
Least-squares matrix: full	23 002 data points
$R_p = 0.056$	Profile function: CW profile function number 4 with 27-terms pseudo-Voigt profile coefficients as parameterized in Thompson *et al.* (1987). Asymmetry correction of Finger *et al.* (1994). Microstrain broadening by Stephens (1999). #1(GU) = 1.163 #2 (GV) = −0.126 #3(GW) = 0.063 #4(GP) = 0.000 #5(LX) = 0.173 #6(ptec) = 0.00 #7 (trns) = 0.00 #8(shft) = 0.0000 #9(sfec) = 0.00 #10(S/L) = 0.0011 #11(H/L) = 0.0011 #12(eta) = 0.8414. Peak tails are ignored where the intensity is below 0.0020 times the peak Aniso. broadening axis 0.0 0.0 1.0.
$R_{wp} = 0.072$	130 parameters
$R_{exp} = 0.068$	79 restraints
$R(F^2) = 0.105\ 38$	$(\Delta/\sigma)_{max} = 0.02$
$\chi^2 = 1.166$	Background function: GSAS background function number 1 with three-terms. Shifted Chebyshev function of first kind 1: 105.356 2: −9.480 73 3: −0.323 215

Fractional atomic coordinates and isotropic displacement parameters (Å^2)

	x	*y*	*z*	U_{iso}
C1	0.8146 (17)	0.6997 (4)	0.7348 (3)	0.0300 (15)
C2	1.0284 (16)	0.5938 (5)	0.7676 (3)	0.0300 (15)
C3	1.0942 (16)	0.5452 (5)	0.8715 (3)	0.0300 (15)
C4	0.9463 (17)	0.6025 (5)	0.9427 (3)	0.0300 (15)
C5	0.7325 (17)	0.7084 (5)	0.9099 (3)	0.0300 (15)
C6	0.6667 (17)	0.7570 (4)	0.8059 (3)	0.0300 (15)
N7	1.2824 (17)	0.4243 (5)	0.9090 (3)	0.0439 (16)
C8	1.503 (2)	0.3763 (6)	0.8490 (4)	0.0439 (16)
C9	1.640 (2)	0.2665 (6)	0.9176 (4)	0.0439 (16)
N10	1.539 (2)	0.2563 (6)	1.0196 (4)	0.0439 (16)
C11	1.323 (2)	0.3507 (6)	1.0108 (3)	0.0439 (16)
C12	1.878 (2)	0.1702 (8)	0.8940 (6)	0.0439 (16)
C13	0.5781 (16)	0.7712 (5)	0.9853 (3)	0.0741 (15)
F14	0.4003 (18)	0.6877 (6)	1.0607 (4)	0.0741 (15)
F15	0.7638 (17)	0.8077 (6)	1.0346 (4)	0.0741 (15)
F16	0.4156 (16)	0.8842 (6)	0.9387 (4)	0.0741 (15)
N17	0.738 57	0.7501	0.630 56	0.0583 (19)
C18	0.734 (2)	0.6788 (4)	0.5672 (4)	0.0583 (19)
O19	0.7976 (17)	0.5571 (4)	0.5935 (5)	0.0261 (19)
C20	0.6158 (17)	0.7539 (5)	0.4637 (3)	0.0244 (11)
C21	0.4752 (17)	0.6827 (5)	0.4172 (4)	0.0244 (11)
C22	0.3670 (16)	0.7495 (5)	0.3202 (3)	0.0244 (11)
C23	0.3994 (16)	0.8874 (5)	0.2696 (3)	0.0244 (11)
C24	0.5400 (15)	0.9586 (4)	0.3161 (4)	0.0244 (11)
C25	0.6482 (16)	0.8919 (5)	0.4131 (4)	0.0244 (11)
C26	0.245 (2)	0.9606 (6)	0.1720 (5)	0.0244 (11)
N27	0.5694 (17)	1.0986 (5)	0.2621 (5)	0.0244 (11)
C28	0.6732 (19)	1.1967 (5)	0.2887 (6)	0.0414 (15)
N29	0.8386 (19)	1.1553 (5)	0.3709 (5)	0.0414 (15)
C30	0.9134 (18)	1.2527 (6)	0.4022 (6)	0.0414 (15)
C31	0.853 (2)	1.3884 (6)	0.3470 (6)	0.0414 (15)
C32	0.687 (2)	1.4183 (5)	0.2631 (6)	0.0414 (15)
N33	0.5857 (19)	1.3244 (5)	0.2339 (5)	0.0414 (15)
C34	1.1122 (18)	1.2099 (6)	0.4889 (6)	0.0404 (16)
C35	1.191 (2)	1.0715 (5)	0.5400 (6)	0.0404 (16)
N36	1.3863 (17)	1.0340 (6)	0.6125 (6)	0.0404 (16)
C37	1.438 (2)	1.1249 (7)	0.6567 (7)	0.0404 (16)
C38	1.328 (2)	1.2564 (7)	0.6203 (7)	0.0404 (16)
C39	1.150 (2)	1.2911 (7)	0.5355(8)	0.0404 (16)

Continued

https://doi.org/10.1017/S0885715615000512 Published online by Cambridge University Press

TABLE I. Continued

H40	1.237 56	0.539 14	0.7147	0.0391 (19)
H41	1.020 06	0.573 22	1.021 71	0.0391 (19)
H42	0.519 97	0.8453	0.777 01	0.0391 (19)
H43	1.556 34	0.418 72	0.767 43	0.057 (2)
H44	1.152 97	0.362 13	1.076 71	0.057 (2)
H45	1.870 74	0.157 24	0.822 47	0.057 (2)
H46	1.808 26	0.054 88	0.956 78	0.057 (2)
H47	2.079 73	0.176 11	0.915 85	0.057 (2)
H48	0.620 63	0.841 04	0.611 81	0.076 (2)
H49	0.451 28	0.566 53	0.459 76	0.0736 (15)
H50	0.250 54	0.685 74	0.287 05	0.0316 (15)
H51	0.767 71	0.942 11	0.443 12	0.0316 (15)
H52	0.109 65	0.878 54	0.154 65	0.0316 (15)
H53	0.418 03	0.981 21	0.0995	0.0316 (15)
H54	0.110 69	1.036 83	0.168 93	0.0316 (15)
H55	0.513 75	1.130 44	0.181 63	0.0316 (15)
H56	0.9071	1.469 53	0.362 67	0.054 (2)
H57	0.646 43	1.5172	0.202 28	0.054 (2)
H58	1.175 65	1.008 34	0.491 61	0.050 (2)
H59	1.283 82	1.305 55	0.683 87	0.052 (2)
H60	1.501 68	1.069 94	0.736 92	0.052 (2)
H61	0.9942	1.394 56	0.529 56	0.052 (2)

TABLE II. DFT (CRYSTAL09) optimized crystal structure of nilotinib.

Crystal data

$C_{28}H_{22}F_3N_7O$	$\beta = 82.1486°$
$M_r = 529.53$	$\gamma = 84.1978°$
Triclinic, $P1$	$V = 607.62$ Å^3
$a = 4.5181$ Å	$Z = 1$
$b = 10.6380$ Å	
$c = 13.7038$ Å	
$\alpha = 68.8607°$	

Fractional atomic coordinates and isotropic displacement parameters (Å^2)

	x	y	z	U_{iso}
C1	0.822 38	0.699 92	0.733 39	0.043 20
C2	1.028 63	0.589 97	0.768 02	0.043 20
C3	1.095 15	0.542 87	0.872 40	0.043 20
C4	0.963 11	0.606 44	0.941 89	0.043 20
C5	0.759 68	0.715 67	0.905 94	0.043 20
C6	0.686 34	0.763 36	0.803 04	0.043 20
N7	1.291 39	0.427 68	0.909 71	0.036 10
C8	1.499 15	0.369 91	0.850 98	0.036 10
C9	1.621 79	0.256 08	0.922 09	0.036 10
N10	1.493 11	0.242 35	1.022 96	0.036 10
C11	1.298 37	0.345 22	1.012 88	0.036 10
C12	1.858 11	0.156 23	0.902 90	0.036 10
C13	0.605 35	0.777 45	0.983 30	0.069 40
F14	0.422 65	0.689 49	1.060 94	0.069 40
F15	0.802 24	0.812 19	1.035 23	0.069 40
F16	0.431 95	0.890 22	0.937 80	0.069 40
N17	0.738 57	0.750 10	0.630 56	0.054 60
C18	0.724 35	0.674 01	0.568 54	0.054 60
O19	0.792 74	0.551 49	0.598 31	0.022 40
C20	0.613 48	0.747 52	0.464 06	0.022 40
C21	0.475 25	0.673 77	0.418 60	0.022 40
C22	0.365 39	0.741 12	0.322 04	0.022 40
C23	0.390 61	0.879 72	0.268 44	0.022 40
C24	0.543 07	0.953 16	0.312 68	0.022 40
C25	0.650 97	0.885 39	0.410 74	0.022 40
C26	0.250 57	0.947 31	0.167 51	0.022 40
N27	0.573 59	1.09 180	0.256 76	0.022 40

Continued

https://doi.org/10.1017/S0885715615000512 Published online by Cambridge University Press

TABLE II. Continued

C28	0.672 73	1.189 11	0.287 02	0.039 90
N29	0.817 09	1.153 51	0.373 01	0.039 90
C30	0.900 69	1.252 03	0.401 26	0.039 90
C31	0.842 21	1.387 88	0.342 15	0.039 90
C32	0.696 98	1.413 92	0.252 80	0.039 90
N33	0.611 31	1.317 76	0.223 67	0.039 90
C34	1.062 47	1.207 71	0.496 35	0.041 60
C35	1.192 53	1.075 99	0.533 42	0.041 60
N36	1.348 14	1.027 76	0.616 91	0.041 60
C37	1.378 02	1.111 00	0.668 45	0.041 60
C38	1.256 28	1.243 28	0.638 65	0.041 60
C39	1.095 95	1.292 76	0.551 37	0.041 60
H40	1.237 56	0.539 14	0.714 70	0.056 20
H41	1.020 06	0.573 22	1.021 71	0.056 20
H42	0.519 97	0.845 30	0.777 01	0.056 20
H43	1.556 34	0.418 72	0.767 43	0.047 00
H44	1.152 97	0.362 13	1.07 671	0.047 00
H45	1.870 74	0.157 24	0.822 47	0.047 00
H46	1.808 26	0.054 88	0.956 78	0.047 00
H47	2.079 73	0.176 11	0.915 85	0.047 00
H48	0.620 63	0.841 04	0.611 81	0.071 00
H49	0.451 28	0.566 53	0.459 76	0.071 00
H50	0.250 54	0.685 74	0.287 05	0.029 00
H51	0.767 71	0.942 11	0.443 12	0.029 00
H52	0.109 65	0.878 54	0.154 65	0.029 00
H53	0.418 03	0.981 21	0.099 50	0.029 00
H54	0.110 69	1.036 83	0.168 93	0.029 00
H55	0.513 75	1.130 44	0.181 63	0.029 00
H56	0.907 10	1.469 53	0.362 67	0.051 90
H57	0.646 43	1.517 20	0.202 28	0.051 90
H58	1.175 65	1.008 34	0.491 61	0.051 90
H59	1.283 82	1.305 55	0.683 87	0.054 00
H60	1.501 68	1.069 94	0.736 92	0.054 00
H61	0.994 20	1.394 56	0.529 56	0.054 00

refining the lattice parameters suggested that the sample may have changed slightly during the measurement.

A density functional geometry optimization (fixed experimental unit cell) was carried out using CRYSTAL09 (Dovesi *et al.*, 2005). The basis sets for the H, C, N, and O atoms were those of Gatti *et al.* (1994), and the basis set for F was that of Nada *et al.* (1993). The calculation used eight *k*-points and the B3LYP functional.

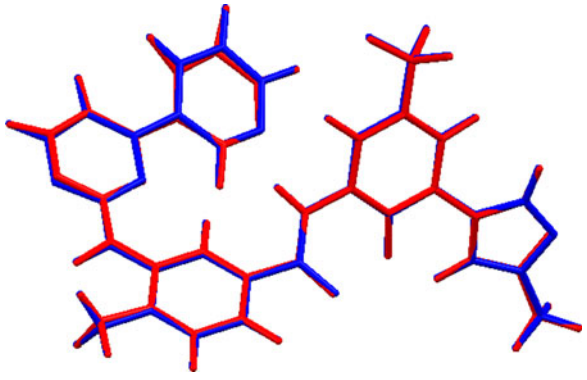

Figure 3. (Color online) Comparison of the refined and optimized structures of nilotinib. The Rietveld refined structure is in red and the DFT-optimized structure is in blue.

III. RESULTS AND DISCUSSION

The refined atom coordinates of nilotinib are reported in Table I, and the coordinates from the DFT optimization in Table II. The root-mean-square deviation of the non-hydrogen atoms is 0.142 Å (Figure 3). The excellent agreement between the refined and optimized structures is strong evidence that the structure is correct (van de Streek and Neumann, 2014). The less-good agreement for the first model serves as a caution that a DFT optimization can merely confirm a false minimum structure. The discussion of the geometry uses the DFT-optimized structure. The asymmetric unit (with atom numbering) is illustrated in Figure 4, and the crystal structure is presented in Figure 5.

All bond distances, angles, and torsion angles fall within the normal ranges indicated by a Mercury Mogul Geometry Check. Nilotinib is generally drawn in an extended conformation, but occurs in the crystal structure in a curled up one. A molecular mechanics conformational analysis in Spartan'14 yields a minimum energy conformation which is even more curled up, having parallel stacking of three 6-rings and another parallel stacking of a 5- and 6-ring. We can then expect that parallel stacking of aromatic rings will be important in the crystal structure, as is observed.

An analysis of the contributions to the total crystal energy using the Forcite module of Materials Studio (Accelrys, 2013) suggests that angle distortion terms are the

https://doi.org/10.1017/S0885715615000512 Published online by Cambridge University Press

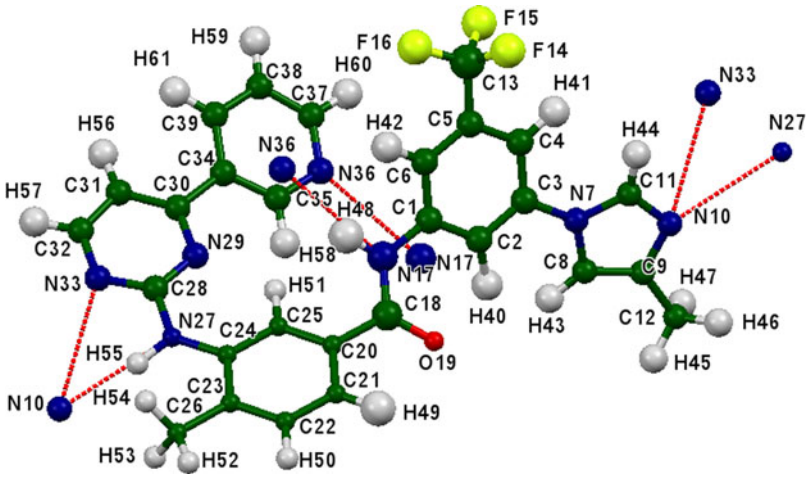

Figure 4. (Color online) The molecular structure of nilotinib, with the atom numbering. The atoms are represented by 50% probability spheroids.

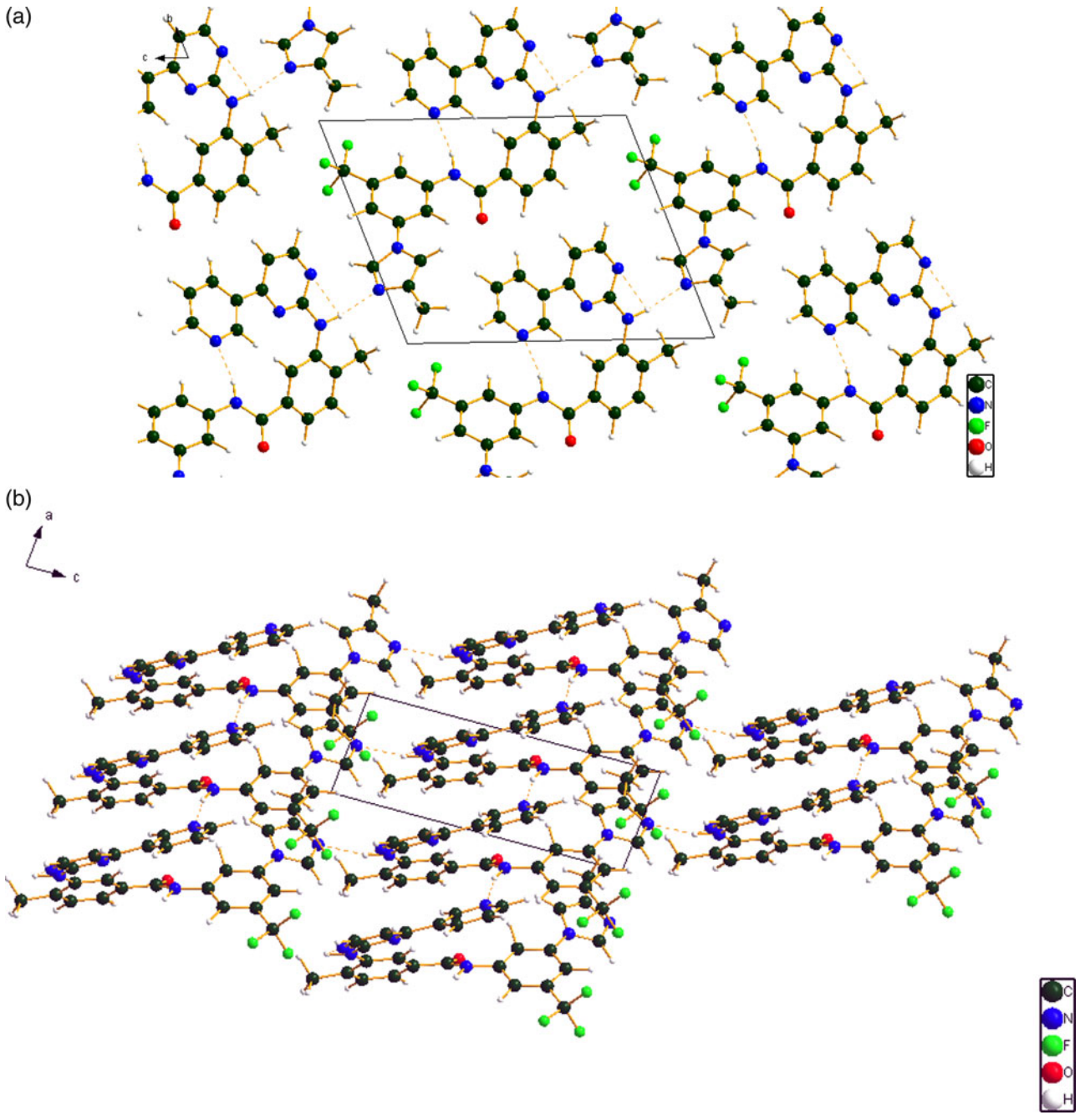

Figure 5. (Color online) (a) The crystal structure of nilotinib, viewed down the *a*-axis. (b) A view down the *b*-axis, showing the parallel stacking of aromatic rings.

https://doi.org/10.1017/S0885715615000512 Published online by Cambridge University Press

TABLE III. Hydrogen bonds in nilotinib.

D–H···A	D–H (Å)	H···A (Å)	D···A (Å)	D–H···A (°)	Overlap (*e*)
N27–H55···N10	1.025	2.078	3.076	163.8	0.061
N17–H48···N36	1.020	2.247	3.242	164.8	0.046
C39–H61···O19	1.085	2.257	3.184	142.1	0.029
C8–H43···O19	1.079	2.403	3.452	163.7	0.027
C21–H49···O19	1.084	2.558	2.845	93.9	0.010

major intramolecular contribution to the crystal energy, and that electrostatic attraction (which in this force field analysis include hydrogen bonds) is important. Van der Waals forces appear to be small. The hydrogen bonds are better analyzed using the results of the DFT calculation.

The most prominent feature of the structure is two strong hydrogen bonds, N27–H55···N10 and N17–H48···N36 (Table III). These form chains with a graph set (Etter, 1990; Bernstein *et al.*, 1995; Shields *et al.*, 2000) *C*1,1(13). The chains run along [111]. Several weak C–H···O hydrogen bonds also contribute to the packing. The carbonyl oxygen O19 acts as an acceptor in both intra- and inter-molecular hydrogen bonds.

The volume enclosed by the Hirshfeld surface (Figure 6; Hirshfeld, 1977; McKinnon *et al.*, 2004; Spackman and Jayatilaka, 2009; Wolff *et al.*, 2012) is 598.58 Å^3, 98.5% of the unit cell volume. The molecules are thus not tightly packed. The only significant close contacts (red in Figure 6) involve the hydrogen bonds.

The Bravais–Friedel–Donnay–Harker (Bravais, 1866; Friedel, 1907; Donnay and Harker, 1937) morphology suggests that we might expect elongated morphology for nilotinib, with <001> as the long axis. A second-order spherical harmonic preferred orientation model was included in the refinement; the texture index was only 1.003, indicating that preferred orientation was not significant for this rotated capillary specimen. The powder pattern of nilotinib has been submitted to ICDD for inclusion in future releases of the PDF.

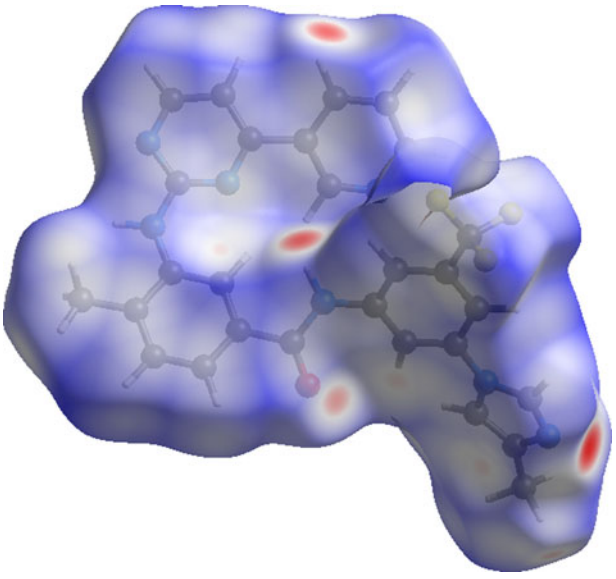

Figure 6. (Color online) The Hirshfeld surface of nilotinib. Intermolecular contacts longer than the sums of the van der Waals radii are colored blue, and contacts shorter than the sums of the radii are colored red. Contacts equal to the sums of radii are white.

SUPPLEMENTARY MATERIALS AND METHODS

The supplementary material for this article can be found at http://www.journals.cambridge.org/PDJ

ACKNOWLEDGEMENTS

Use of the Advanced Photon Source at Argonne National Laboratory was supported by the U.S. Department of Energy, Office of Science, Office of Basic Energy Sciences, under Contract No. DE-AC02-06CH11357. This work was partially supported by the International Centre for Diffraction Data. The authors thank Lynn Ribaud for his assistance in data collection and Thanh Nguyen and Gerry Zajac of Ineos Technologies for the chemical analysis.

Accelrys (**2013**). *Materials Studio 7.0* (Accelrys Software Inc., San Diego, California).

Allen, F. H. (**2002**). "The Cambridge Structural Database: a quarter of a million crystal structures and rising," Acta Crystallogr. B, Struct. Sci. **58**, 380–388.

Altomare, A., Cuocci, C., Giacovazzo, C., Moliterni, A., Rizzi, R., Corriero, N., and Falcicchio, A. (**2013**). "EXPO2013: a kit of tools for phasing crystal structures from powder data", J. Appl. Crystallogr. **46**, 1231–1235.

Bernstein, J., Davis, R. E., Shimoni, L., and Chang, N. L. (**1995**). "Patterns in hydrogen bonding: functionality and graph set analysis in crystals," Angew. Chem. Int. Ed. Engl. **34**(15), 1555–1573.

Bravais, A. (**1866**). *Etudes Cristallographiques* (Gauthier Villars, Paris).

Bruno, I. J., Cole, J. C., Kessler, M., Luo, J., Motherwell, W. D. S., Purkis, L. H., Smith, B. R., Taylor, R., Cooper, R. I., Harris, S. E., and Orpen, A. G. (**2004**). "Retrieval of crystallographically-derived molecular geometry information," J. Chem. Inf. Sci. **44**, 2133–2144.

Deremer, D. L., Ustun, C., and Natarajan, K. (**2008**). "Nilotinib: a second-generation tyrosine kinase inhibitor for the treatment of chronic myelogenous leukemia," Clin. Ther. **30**(11), 1956–1975.

Donnay, J. D. H. and Harker, D. (**1937**). "A new law of crystal morphology extending the law of Bravais," Am. Mineral. **22**, 446–467.

Dovesi, R., Orlando, R., Civalleri, B., Roetti, C., Saunders, V. R., and Zicovich-Wilson, C. M. (**2005**). "CRYSTAL: a computational tool for the *ab initio* study of the electronic properties of crystals," Z. Kristallogr. **220**, 571–573.

Etter, M. C. (**1990**). "Encoding and decoding hydrogen-bond patterns of organic compounds," Acc. Chem. Res. **23**(4), 120–126.

Favre-Nicolin, V. and Černý, R. (**2002**). "FOX, free objects for crystallography: a modular approach to *ab initio* structure determination from powder diffraction," J. Appl. Crystallogr. **35**, 734–743.

Finger, L. W., Cox, D. E., and Jephcoat, A. P. (**1994**). "A correction for powder diffraction peak asymmetry due to axial divergence," J. Appl. Crystallogr. **27**(6), 892–900.

Friedel, G. (**1907**). "Etudes sur la loi de Bravais," Bull. Soc. Fr. Mineral. **30**, 326–455.

Gatti, C., Saunders, V. R., and Roetti, C. (**1994**). "Crystal-field effects on the topological properties of the electron-density in molecular crystals – the case of urea," J. Chem. Phys. **101**, 10686–10696.

Hirshfeld, F. L. (**1977**). "Bonded-atom fragments for describing molecular charge densities," Theor. Chem. Acta **44**, 129–138.

https://doi.org/10.1017/S0885715615000512 Published online by Cambridge University Press

ICDD (**2014**). *PDF-4 + 2014 (Database)*, edited by S. Kabekkodu (International Centre for Diffraction Data, Newtown Square, PA).

Larson, A. C. and Von Dreele, R. B. (**2004**). *General Structure Analysis System (GSAS)*, (Report LAUR 86-784). Los Alamos, New Mexico: Los Alamos National Laboratory.

Lee, P. L., Shu, D., Ramanathan, M., Preissner, C., Wang, J., Beno, M. A., Von Dreele, R. B., Ribaud, L., Kurtz, C., Antao, S. M., Jiao, X., and Toby, B. H. (**2008**). "A twelve-analyzer detector system for high-resolution powder diffraction," J. Synchrotron Radiat. **15**(5), 427–432.

Louër, D. and Boultif, A. (**2007**). "Powder pattern indexing and the dichotomy algorithm," Z. Kristallogr. Suppl. **2007**, 191–196.

McKinnon, J. J., Spackman, M. A., and Mitchell, A. S. (**2004**). "Novel tools for visualizing and exploring intermolecular interactions in molecular crystals," Acta Crystallogr. B **60**, 627–668.

Nada, R., Catlow, C. R. A., Pisani, , and Orlando, R. (**1993**). "Ab initio Hartree-Fock perturbed-cluster study of neutral defects in LiF," Model. Simul. Mater. Sci. Eng. **1**, 165–187.

O'Boyle, N., Banck, M., James, C. A., Morley, C., Vandermeersch, and Hutchison, G. R. (**2011**). "Open Babel: an open chemical toolbox," J. Chem. Inf. **3**, 33.

Shields, G. P., Raithby, P. R., Allen, F. H., and Motherwell, W. S. (**2000**). "The assignment and validation of metal oxidation states in the Cambridge Structural Database," Acta Crystallogr. B, Struct. Sci. **56**(3), 455–465.

Spackman, M. A. and Jayatilaka, D. (**2009**). "Hirshfeld surface analysis," CrystEngComm. **11**, 19–32.

Stephens, P. W. (**1999**). "Phenomenological model of anisotropic peak broadening in powder diffraction," J. Appl. Crystallogr. **32**, 281–289.

Sykes, R. A., McCabe, P., Allen, F. H., Battle, G. M., Bruno, I. J., and Wood, P. A. (**2011**). "New software for statistical analysis of Cambridge Structural Database data," J. Appl. Crystallogr. **44**, 882–886.

Thompson, P., Cox, D. E., and Hastings, J. B. (**1987**). "Rietveld refinement of Debye–Scherrer synchrotron X-ray data from Al_2O_3," J. Appl. Crystallogr. **20**(2), 79–83.

van de Streek, J. and Neumann, M. A. (**2014**). "Validation of molecular crystal structures from powder diffraction data with dispersion-corrected density functional theory (DFT-D)," Acta Crystallogr. B, Struct. Sci., Cryst. Eng. Mater. **70**(6), 1020–1032.

Wang, J., Toby, B. H., Lee, P. L., Ribaud, L., Antao, S. M., Kurtz, C., Ramanathan, M., Von Dreele, R. B., and Beno, M. A. (**2008**). "A dedicated powder diffraction beamline at the advanced photon source: commissioning and early operational results," Rev. Sci. Instrum. **79**, 085105.

Wavefunction, Inc. (**2013**). *Spartan'14 Version 1.1.0* (Wavefunction Inc., Irvine, California).

Wolff, S. K., Grimwood, D. J., McKinnon, M. J., Turner, M. J., Jayatilaka, D., and Spackman, M. A. (**2012**). *CrystalExplorer Version 3.1* (University of Western Australia, Perth, Australia).

https://doi.org/10.1017/S0885715615000512 Published online by Cambridge University Press